

# Multi-Shot Mining Semantic Part Concepts in CNNs

Quanshi Zhang, Ruiming Cao, Ying Nian Wu, and Song-Chun Zhu

University of California, Los Angeles

## Abstract

This paper proposes a new learning strategy that incrementally embeds new object-part concepts into a pre-trained convolutional neural network (CNN), in order to 1) explore explicit semantics for the CNN units and 2) gradually transfer the pre-trained CNN into a “white-box” model for hierarchical object understanding. Given part annotations on a very small number (*e.g.* 3–12) of objects, our method mines certain units from the pre-trained CNN and associate them with different part concepts. We use a four-layer And-Or graph to organize the CNN units, which clarifies their internal semantic hierarchy. Our method is guided by a small number of part annotations, and it achieves superior part-localization performance (about 28%–107% improvement in part center prediction).

## Introduction

Due to the development of convolutional neural networks (LeCun et al. 1998; Krizhevsky, Sutskever, and Hinton 2012) (CNNs), object detection methods have achieved near human-level performance. However, in real-world applications, we are still facing two important issues.

First, many tasks have gone beyond the detection of object bounding boxes, and required detailed structural knowledge of an object. Thus, hierarchical understanding of object components (*e.g.* part localization and parsing) has received an increasing attention in recent years. Second, unlike data-rich applications (*e.g.* pedestrian and vehicle detection), many visual tasks are usually based on “temporary” demands for modeling certain objects or even certain parts on objects (*e.g.* teaching a robot to identify and grasp a certain part on a class of objects). People mainly train object-level models for daily-use categories, but people cannot pre-know target parts before each specific task or have enough time to annotate sufficient training samples.

Therefore, in this study, we hope to use very few annotations to add new part concepts into a CNN that is pre-trained to represent “entire objects.” We grow a semantic branch on the CNN to encode each part concept and achieve hierarchical object understanding. We will introduce this learning strategy from the following three perspectives.

Copyright © 2017, Association for the Advancement of Artificial Intelligence (www.aaai.org). All rights reserved.

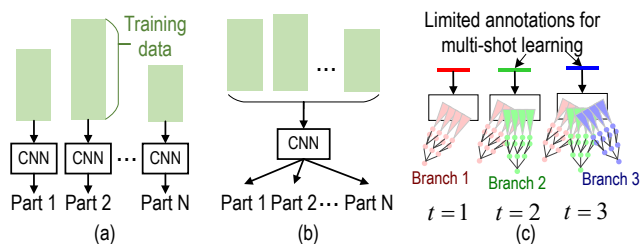


Figure 1: Comparison of batch learning strategies. (a) Individually learning/fine-tuning each part without sharing patterns between parts has great information redundancy in model representation. (b) Jointly learning/fine-tuning parts requires all parts to be simultaneously learned. (c) Given a temporary demand for modeling a new part and a small number (*e.g.* 3–12) of part annotations at time  $t$ , we incrementally grow neural connections to the part, and build a new semantic branch on a pre-trained CNN.

**Perspective 1, incremental growth of neural connections:** As reported in (Kumaran, Hassabis, and McClelland 2016), there are “two learning systems instantiated in mammals:” 1) the neocortex gradually acquires sophisticated knowledge representation, and 2) the hippocampus quickly learns specifics of individual experiences. CNNs are typically trained using big data to represent entire objects. We can parallel CNNs to the neocortex; they contain rich appearance patterns. Then, given a demand for modeling a certain part, we quickly transfer patterns in the CNNs to the part, which corresponds to the short-term learning in hippocampus.

*Given a pre-trained CNN and a target part concept, our method builds new connections between certain CNN units and this part concept, in order to incrementally enrich part concepts in the CNN for hierarchical object understanding.*

It is important to maintain the generality of the pre-trained CNN during the learning procedure. *I.e.* we do not change/fine-tune the original convolutional weights within the CNN, when we grow neural connections. This allows us to continuously add new part concepts to the same CNN, without worrying about the model drift problem.

**Perspective 2, multi-shot learning from small data:** As shown in Fig. 1, our method requires much less (*e.g.* 3–12) part annotations than conventional supervised approaches.

**Perspective 3, CNN semanticization:** Because a CNN

unit naturally corresponds to a latent visual pattern, in recent years, people have exhibited a special interest in opening the black-box representation of the CNN. In our research, the learning procedure is actually to retrieve “implicit” patterns from the CNN, and associate them with “explicit” part concepts. Thus, we obtain an interpretable representation of CNN patterns, which may contribute to the understanding of knowledge organization in the CNN. The semanticized patterns can be transferred from the CNNs to different applications, *e.g.* part localization in this study.

**Task inputs and outputs:** Given a pre-trained CNN and a number of images for a certain category, we only annotate semantic parts on a few images as inputs. We develop a method to grow an And-or graph (AoG) as a side branch of the pre-trained CNN, which associates certain CNN units with the part concept. Our method does not require massive annotations for learning, and can be conducted with even a **single** part annotation. We can use the learned AoG to parse/localize object parts and their compositional subpart regions to enable hierarchical object understanding.

As shown in Fig. 2, the target AoG has a four-layer semantic hierarchy ranging from *semantic parts* (OR nodes), *appearance candidates* (AND nodes), *latent patterns* (OR nodes), and *CNN units* (terminal nodes). In the AoG, we use OR nodes to represent alternative appearance patterns of a certain part/region, and use AND nodes to represent a region’s sub-part components, as follows. The top node of a *semantic part* (*e.g.* a head, OR node) lists a number of (contextual) appearance candidates as children, which may appear with different poses. An *appearance candidate* (AND node) has a number of children latent patterns to represent its sub-regions. A *latent pattern* (OR node) naturally corresponds to a certain range of units within a CNN conv-slice. It selects a *CNN unit* within this range to account for local shape deformation of this pattern. When we build the AoG, we hope each node in the AoG can represent both the specific appearance of a few annotated samples and common knowledge among the large number of unannotated images, to avoid the over-fitting problem.

**Contributions** of this paper are summarized as follows.

- 1) From the perspective of model learning, given a few part annotations, we propose a new learning strategy that is able to incrementally grow new neural connections to gradually add new part concepts into a pre-trained CNN.
- 2) From the perspective of knowledge transferring, our method semanticizes the CNN by associating implicit object-level patterns in the CNN with explicit part concepts and revealing their semantic structures.
- 3) To the best of our knowledge, we can regard our method as the first study to achieve weakly supervised (*e.g.* 3–12 annotations) learning for part localization. Our method exhibits superior localization performance in experiments (about 28%–107% improvement in part center prediction).

## Related work

**Modeling “objects” vs. modeling “parts” in un-/weakly-supervised learning:** Generally speaking, in the scope of un-/weakly-supervised learning, modeling parts is usually more challenging than modeling entire objects. Given

image-level labels (without object bounding boxes), object discovery (Oquab et al. 2015; Simon and Rodner 2015; Darrell 2015) can be achieved by identifying common foreground patterns from chaotic background. Closed boundaries and common object structure are also strong prior knowledge for object discovery (Zhang, Wu, and Zhu 2015).

In contrast, there is no mechanism to automatically distinguish a certain part concept from other common foreground patterns. In addition, some parts (*e.g.* the abdomen) do not have shape boundaries to determine their shape extent.

**Semantics in the CNN:** In order to explore the hidden semantics in the CNN, many studies have focused on the visualization of CNN units (Zeiler and Fergus 2014; Mahendran and Vedaldi 2015; Simonyan, Vedaldi, and Zisserman 2013; Dosovitskiy and Brox 2015; Aubry and Russell 2015) and analyzed their statistical features (Dosovitskiy et al. 2014; Szegedy et al. 2014; Yosinski et al. 2014; Lu 2015). Liu et al. (Liu, Shen, and van den Hengel 2015) extracted and visualized a subspace of CNN features.

However, going beyond the “passive” visualization, some studies “actively” extracted CNN units with certain semantics for different applications. Zhou *et al.* (Zhou et al. 2015; Zhou et al. 2016) discovered latent “scene” semantics from CNN feature maps. Simon *et al.* discovered objects (Simon and Rodner 2015) in an unsupervised manner from CNN feature maps, and learned part concepts in a supervised fashion (Simon, Rodner, and Denzler 2014). In this study, given a very few part annotations, we mine CNN patterns that are related to the part concept. Obtaining clear semantics makes it easier to transfer CNN patterns to other part-based tasks.

**Knowledge transferring:** Transferring hidden patterns in the CNN to other tasks is important for neural networks. Typical research includes end-to-end fine-tuning and transferring CNN knowledge between different categories (Yosinski et al. 2014; Gallagher, Tang, and Tu 2015) and/or datasets (Ganin and Lempitsky 2015). In contrast, we believe that a good explanation and transparent representation of part knowledge will create a new possibility of transferring part knowledge. As in (Zhu et al. 2008; Si and Zhu 2013), the AoG is suitable to represent the semantic hierarchy, which enables semantic-level interactions between human and neural networks.

**Part localization/detection vs. semanticizing CNN patterns:** Part localization/detection is a fundamental problem in computer vision (Azizpour and Laptev 2012; Simon, Rodner, and Denzler 2014; Li et al. 2013; Chen et al. 2014). There are two key points to differentiate our study from conventional part-detection approaches. First, most methods for detection, such as the CNN and the DPM (LeCun et al. 1998; Felzenszwalb, Girshick, and McAllester 2010; Tsogkas et al. 2015), limit their attention to the classification problem. In contrast, our effort is to clarify semantic meanings of chaotic CNN patterns. Second, instead of summarizing knowledge from massive annotations, our method mines CNN semantics with very limited supervision.

## And-Or graph for part parsing

In this section, we introduce the structure of the AoG and part parsing/localization based on the AoG. The method for

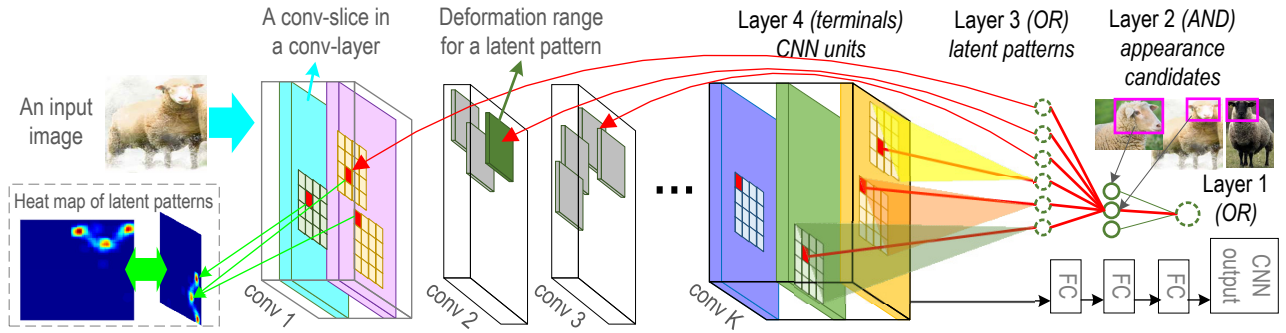


Figure 2: And-Or graph as a semantic branch grown on the pre-trained CNN. The AoG associates CNN units with certain part (head, here) concepts. Red lines in the AoG indicate a parse graph for concept association. To visualize these latent patterns, we show the heat map (left) at the 5-th conv-layers in the VGG-16 network, which sums up the associated units (red squares) throughout all conv-slices. In Fig. 4, we reconstructed the dog head using the learned AoG to show its interpretability.

AoG construction will be introduced in the next section. As shown in Fig. 2, an AoG represents a part’s semantic structure at four layers, *i.e.* *semantic part* (OR node), *appearance candidate* (AND node), *latent pattern* (OR node), and *CNN unit*. We use  $V^{\text{sem}}, V^{\text{app}} \in \Omega^{\text{app}}, V^{\text{lat}} \in \Omega^{\text{lat}}$ , and  $V^{\text{unt}} \in \Omega^{\text{unt}}$ , respectively, to denote nodes at the four layers. Each OR node in the AoG represents a list of alternative appearance (or deformation) candidates. Each AND node encodes a number of latent patterns to describe its sub-regions.

Given CNN activation maps on an image  $I^1$ , we can use the AoG for part parsing to produce a hierarchical part understanding. From a top-down perspective, the parsing procedure 1) detects the target part and identifies its corresponding appearance candidate; 2) for each latent pattern under the appearance candidate, it selects a CNN unit within a certain deformation range as a stand-in of this pattern. In this way, we parse an image region for each AoG node.

As red lines in Fig. 2, we use a parse graph  $pg_I$  to denote the parsing result. A parse graph  $pg_I$  consists of a tree of region inferences  $pg = \{\Lambda_{I, V^{\text{sem}}}\} \cup_{V^{\text{lat}} \in \text{Child}(\hat{V}^{\text{app}})} \{\Lambda_{I, V^{\text{lat}}}\}$ , where  $\hat{V}^{\text{app}}$  denotes the appearance candidate that is selected for image  $I$ . We parse an image region within  $I$  for each node  $V$ , given as  $\Lambda_{I, V} = (\mathbf{P}_{I, V}, \mathbf{S}_{I, V})$ .  $\mathbf{P}_{I, V}$  and  $\mathbf{S}_{I, V}$  denote the center and scale of  $\Lambda_{I, V}$ . Without ambiguity, we use  $\mathbf{P}_V$  and  $\mathbf{S}_V$ , respectively, to simplify the notation. Because the region scale  $\mathbf{S}_V$  can be easily determined (which will be introduced in following paragraphs), we simply use the central position  $\mathbf{P}_V$  to represent the region  $\Lambda_{I, V}$  for clarity.

Part parsing is achieved in a bottom-up manner, as follows. We design a generative inference score  $S_I(V|\mathbf{P}_V)$  for each AoG node  $V$ , in order to measure the fitness between a given region  $\mathbf{P}_V$  and  $V$  (as well as the sub-AoG under  $V$ ). We propagate generative scores from terminal CNN units in a bottom-up fashion, and finally obtain the score of the top AoG node as the overall generative score. We estimate the parse graph  $\hat{pg}_I$  that maximizes the overall generative score.

$$\mathbf{L}^{\text{gen}}(I, \theta) = S_I(V^{\text{sem}}|\mathbf{P}_{V^{\text{sem}}}), \quad \hat{pg}_I = \underset{pg_I}{\text{argmax}} \mathbf{L}^{\text{gen}}(I, \theta)|_{pg_I(1)}$$

<sup>1</sup>Because the CNN has demonstrated its superior performance in object detection, we assume that the target object can be well detected by the pre-trained CNN. Thus, to simplify the learning scenario, we crop  $I$  to only contain the object, resize it to the image size for CNN inputs, and only focus on the part localization task.

where  $S_I(V^{\text{sem}}|\mathbf{P}_{V^{\text{sem}}})$  measures the score of the entire semantic part on image  $I$ ;  $\theta$  denotes the AoG parameters.

**Score propagation for OR nodes:** Each OR node  $V^O$  (either a semantic part  $V^{\text{sem}}$  or a latent pattern  $V^{\text{lat}}$ ) contains a list of alternative patterns. Given the parsed region of each child pattern  $V, \hat{\mathbf{P}}_V$ , as input, we select the child  $\hat{V}$  with the highest score as the true parsing configuration:

$$S_I(V^O|\hat{\mathbf{P}}_{V^O}) = \max_{V \in \text{Child}(V^O)} S_I(V|\hat{\mathbf{P}}_V), \quad \hat{\mathbf{P}}_{V^O} = \hat{\mathbf{P}}_{\hat{V}}, \quad \hat{\mathbf{S}}_{V^O} = \hat{\mathbf{S}}_{\hat{V}} \quad (2)$$

In details, the OR node of the semantic part has a number of appearance candidates as children. The OR node of a latent pattern  $V^{\text{lat}}$  encodes a number of CNN units which represent different deformation candidates.  $V^{\text{lat}}$  is represented using parameters  $\{L_{V^{\text{lat}}}, D_{V^{\text{lat}}}, \bar{\mathbf{P}}_{V^{\text{lat}}}, \Delta\mathbf{P}_{V^{\text{lat}}}\} \subset \theta$ . It means that a latent pattern  $V^{\text{lat}}$  naturally corresponds to a square within a certain conv-slice (the  $D_{V^{\text{lat}}}$ -th depth/channel in the output of the  $L_{V^{\text{lat}}}$ -th CNN conv-layer) as its deformation range<sup>2</sup>.  $V^{\text{lat}}$  connects all the CNN units within the deformation range as different location candidates.  $\bar{\mathbf{P}}_{V^{\text{lat}}}$  denotes the image position corresponding to the square center. We regard  $\bar{\mathbf{P}}_{V^{\text{lat}}}$  as  $V^{\text{lat}}$ ’s “ideal” position without any deformation. For each  $V^{\text{lat}}$ ,  $\Delta\mathbf{P}_{V^{\text{lat}}}$  denotes the average displacement from its ideal position  $\bar{\mathbf{P}}_{V^{\text{lat}}}$  to its parent’s region  $\mathbf{P}_{V^{\text{app}}}$ .

**Score propagation for AND nodes:** The AND node of an appearance candidate  $V^{\text{app}}$  models the relationship between a certain part appearance and its sub-regions. We select children latent patterns from a total of  $K$  conv-layers to represent the sub-regions. We select  $n_k$  latent patterns from the  $k$ -th ( $k = 1, 2, \dots, K$ ) conv-layer, where  $\{n_k\}$  are hyper-parameters. The scale of  $V^{\text{app}}$ ’s image region  $\mathbf{S}_{V^{\text{app}}}$  is simply computed using part annotations, which will be introduced in the next section. Given parsing results of children patterns  $\{\hat{\mathbf{P}}_{V^{\text{lat}}}\}$ , we use the following generative inference score to predict the region center of  $V^{\text{app}}$ .

$$S_I(V^{\text{app}}|\mathbf{P}_{V^{\text{app}}}) = \sum_{V^{\text{lat}} \in \text{Child}(V^{\text{app}})} [S_I(V^{\text{lat}}|\hat{\mathbf{P}}_{V^{\text{lat}}}) + S^{\text{inf}}(\mathbf{P}_{V^{\text{app}}}|\hat{\mathbf{P}}_{V^{\text{lat}}})] \quad (3)$$

$$\hat{\mathbf{P}}_{V^{\text{app}}} = \underset{\mathbf{P}_{V^{\text{app}}}}{\text{argmax}} S_I(V^{\text{app}}|\mathbf{P}_{V^{\text{app}}})$$

First, in the above equation,  $S_I(V^{\text{lat}}|\hat{\mathbf{P}}_{V^{\text{lat}}})$  is the inference score of child  $V^{\text{lat}}$ , which has already been computed.

<sup>2</sup>We set a constant deformation range for each latent pattern, which potentially covers  $75 \times 75$  pxls on the image. Deformation ranges of different patterns in the same conv-slice may overlap.

Second, we can use  $V^{\text{lat}}$ 's region to infer  $V^{\text{app}}$ 's region, because we record the displacement  $\Delta \mathbf{P}_{V^{\text{lat}}}$  between them.  $S_I^{\text{inf}}(\mathbf{P}_{V^{\text{app}}}|\hat{\mathbf{P}}_{V^{\text{lat}}})^3$  measures spatial compatibility between  $V^{\text{app}}$  and each child  $V^{\text{lat}}$  in region parsing.

**Terminal nodes (CNN units)**  $V^{\text{unt}}$  under a latent pattern are deformation candidates of this latent pattern.  $V^{\text{unt}}$  has a fixed image region  $\Lambda_{I,V^{\text{unt}}} = (\mathbf{S}_{V^{\text{unt}}}, \mathbf{P}_{V^{\text{unt}}})$ : we propagate the receptive field of  $V^{\text{unt}}$  back to the image plane as  $\Lambda_{I,V^{\text{unt}}}$ . The generative score of  $V^{\text{unt}}$  is given as

$$S_I(V^{\text{unt}}|\mathbf{P}_{V^{\text{unt}}}) = S_I^{\text{rsp}}(V^{\text{unt}}) + S_I^{\text{loc}}(V^{\text{unt}}) + S_I^{\text{pair}}(V^{\text{unt}}) \quad (4)$$

The above score consists of the following three terms: 1)  $S_I^{\text{rsp}}(V^{\text{unt}})^3$  denotes the response value of the unit  $V^{\text{unt}}$ , when we input image  $I$  into the CNN. 2) When the parent  $V^{\text{lat}}$  selects  $V^{\text{unt}}$  as its location inference (*i.e.*  $\hat{\mathbf{P}}_{V^{\text{lat}}} \leftarrow \mathbf{P}_{V^{\text{unt}}}$ ),  $S_I^{\text{loc}}(V^{\text{unt}})^3$  measures the deformation level between  $V^{\text{unt}}$ 's location and  $V^{\text{lat}}$ 's ideal location  $\bar{\mathbf{P}}_{V^{\text{lat}}}$ . 3)  $S_I^{\text{pair}}(V^{\text{unt}})$  indicates the spatial compatibility between neighboring latent patterns: we model the pairwise spatial relationship between latent patterns in the upper conv-layer and those in the current conv-layer. For each  $V^{\text{unt}}$  (with its parent  $V^{\text{lat}}$ ) in conv-layer  $L_{V^{\text{lat}}}$ , we select 5 nearest latent patterns in conv-layer  $L_{V^{\text{lat}}} + 1$ , *w.r.t.*  $\|\bar{\mathbf{P}}_{V^{\text{lat}}} - \bar{\mathbf{P}}_{V^{\text{lat}}_{\text{upper}}}\|$ , as the neighboring latent patterns. Please see the section of appendix for details of  $S_I^{\text{rsp}}(V^{\text{unt}})$ ,  $S_I^{\text{loc}}(V^{\text{unt}})$ , and  $S_I^{\text{pair}}(V^{\text{unt}})$ .

**Hierarchical part parsing/localization based on the AoG:** Given an image  $I^1$  and an AoG, the concept association problem in (1) can be solved by dynamic programming in a bottom-up manner. Note that we first infer latent patterns corresponding to high conv-layers, and use the inference results to select units in low conv-layers.

## And-Or graph construction

**Training data:** Let  $\mathbf{I}$  denote an image set for a target category. Among all objects in  $\mathbf{I}$ , we label bounding boxes of the semantic part in a small number of images,  $\mathbf{I}^{\text{ant}} = \{I_i | i = 1, 2, \dots, M\} \subset \mathbf{I}$ . In addition, we manually define a number of appearance candidates for the part. Thus, for each  $I \in \mathbf{I}^{\text{ant}}$ , we annotate  $(\Lambda_{I,V^{\text{sem}}}^*, V^{\text{app}*})$ , where  $\Lambda_{I,V^{\text{sem}}}^* = (\mathbf{S}_{V^{\text{sem}}}^*, \mathbf{P}_{V^{\text{sem}}}^*)$  denotes the ground-truth bounding box of the part in  $I$ , and  $V^{\text{app}*}$  specifies the ground-truth appearance type for the part.

**Which AoG parameters to learn:** We can use human annotations to manually define the first two layers of the AoG. If people specify a total of  $m$  different types of part appearance during the annotation process, correspondingly, we can directly connect the top node with  $m$  appearance candidates  $\{V^{\text{app}*}\}$  as children. For each appearance candidate  $V^{\text{app}}$ , let  $\bar{\mathbf{P}}_{V^{\text{app}}}^*$  and  $\bar{\mathbf{S}}_{V^{\text{app}}}^*$  denote the average position and scale among all part boxes that are annotated for  $V^{\text{app}}$ . We set  $V^{\text{app}}$  with a constant scale  $\mathbf{S}_{V^{\text{app}}} = \bar{\mathbf{S}}_{V^{\text{app}}}^*$ .

Thus, the key of AoG construction is to mine latent patterns for each appearance candidate. We need to select a total of  $n_k$  different latent patterns from the  $k$ -th ( $k = 1, 2, \dots, K$ ) conv-layer of the CNN. Each of these latent patterns is defined by its location parameters  $\{L_{V^{\text{lat}}}, D_{V^{\text{lat}}}, \bar{\mathbf{P}}_{V^{\text{lat}}}, \Delta \mathbf{P}_{V^{\text{lat}}}\} \subset \theta$ . Each  $V^{\text{lat}}$  in the  $k$ -th conv-layer has a fixed value of  $L_{V^{\text{lat}}} = k$ . Given parameter  $\bar{\mathbf{P}}_{V^{\text{lat}}}$ ,

<sup>3</sup>These scores are simply formulated based on the original or squared difference. Please see the section of appendix for details.

the displacement  $\Delta \mathbf{P}_{V^{\text{lat}}}$  between  $V^{\text{lat}}$  and its parent  $V^{\text{app}}$  can be computed as  $\Delta \mathbf{P}_{V^{\text{lat}}} = \mathbf{P}_{V^{\text{app}}}^* - \bar{\mathbf{P}}_{V^{\text{lat}}}$ . As a result, we only need to learn the conv-slice  $D_{V^{\text{lat}}}$  and central position  $\bar{\mathbf{P}}_{V^{\text{lat}}}$  for each of the  $n_k$  latent patterns.

**How to learn:** We mine the latent patterns by estimating their best locations  $D_{V^{\text{lat}}}$  and  $\bar{\mathbf{P}}_{V^{\text{lat}}}$  that maximize the following objective function.

$$\max_{\theta} \left\{ \frac{1}{M} \sum_{I \in \mathbf{I}^{\text{ant}}} \left[ \mathbf{L}^{\text{gen}}(I, \theta) |_{\hat{p}g_I} + \mathbf{L}^{\text{dis}}(\hat{\mathbf{P}}_{V^{\text{sem}}}, \mathbf{P}_{V^{\text{sem}}}^* | I) \right] + \sum_{V^{\text{lat}} \in \Omega^{\text{lat}}} \left[ S^{\text{close}}(V^{\text{lat}}) + \text{mean}_{I' \in \mathbf{I}} \lambda^{\text{common}} \max_{\mathbf{P}_{V^{\text{lat}}}} S_{I'}(V^{\text{lat}} | \mathbf{P}_{V^{\text{lat}}}) \right] \right\} \quad (5)$$

First, let us focus on the first half of the equation. We consider both the generative inference score  $\mathbf{L}^{\text{gen}}(I, \theta)$  on  $I$  (defined in (1)) and its discriminative score  $\mathbf{L}^{\text{dis}}(\hat{\mathbf{P}}_{V^{\text{sem}}}, \mathbf{P}_{V^{\text{sem}}}^* | I)$ . Based on (1), given annotations  $(\mathbf{P}_{V^{\text{sem}}}^*, V^{\text{app}*})$  for image  $I$ , we can obtain  $\mathbf{L}^{\text{gen}}(I, \theta) |_{\hat{p}g_I} = S_I(V^{\text{sem}} | \hat{\mathbf{P}}_{V^{\text{sem}}}) = S_I(V^{\text{app}*} | \hat{\mathbf{P}}_{V^{\text{app}*}})$ . The discriminative score measures the localization error between the predicted part region  $\hat{\mathbf{P}}_{V^{\text{sem}}}$  and the ground truth  $\mathbf{P}_{V^{\text{sem}}}^*$ . We define

$$\mathbf{L}^{\text{dis}}(\hat{\mathbf{P}}_{V^{\text{sem}}}, \mathbf{P}_{V^{\text{sem}}}^* | I) = -\lambda_{V^{\text{app}*}} \|\hat{\mathbf{P}}_{V^{\text{sem}}} - \mathbf{P}_{V^{\text{sem}}}^*\|^2 \quad (6)$$

We ignore the small probability of the AoG assigning an annotated image with an incorrect appearance candidate to simplify the computation, *i.e.*  $\hat{V}^{\text{app}} \equiv V^{\text{app}*}$ ,  $\hat{\mathbf{P}}_{V^{\text{sem}}} \equiv \mathbf{P}_{V^{\text{app}*}}$ .

Second, in the second half of (5),  $S^{\text{close}}(V^{\text{lat}})^3$  measures the spatial closeness between a latent pattern  $V^{\text{lat}}$  and its parent  $V^{\text{app}}$ , because latent patterns spatially closer to  $V^{\text{app}}$  are usually more reliable. The last term measures the prior commonness of  $V^{\text{lat}}$  among all objects (including objects without part annotations). We assume that latent patterns that frequently appear among all images may potentially represent stable sub-part semantics and should have higher priorities.

When we set  $\lambda_{V^{\text{app}*}}$  to a constant  $\lambda^{\text{inf}} \sum_{k=1}^K n_k$ , we can transform the learning objective in (5) as follows (please see supplementary materials for the proof).

$$\forall V^{\text{app}} \in \Omega^{\text{app}}, \quad \max_{\theta_{V^{\text{app}}}} \sum_{V^{\text{lat}} \in \text{Child}(V^{\text{app}})} \text{Score}(V^{\text{lat}}) \quad (7)$$

where  $\text{Score}(V^{\text{lat}}) = \frac{1}{M} \sum_{I \in \mathbf{I}_{V^{\text{app}}}} [S_I(V^{\text{lat}} | \hat{\mathbf{P}}_{V^{\text{lat}}}) + S_I^{\text{inf}}(\mathbf{P}_{V^{\text{sem}}}^* | \hat{\mathbf{P}}_{V^{\text{lat}}}) + S^{\text{close}}(V^{\text{lat}}) + \lambda^{\text{common}} \text{mean}_{I' \in \mathbf{I}} \max_{\mathbf{P}_{V^{\text{lat}}}} S_{I'}(V^{\text{lat}} | \mathbf{P}_{V^{\text{lat}}})]$ .  $\theta_{V^{\text{app}}} \subset \theta$  denotes the parameters for the sub-AoG of  $V^{\text{app}}$ . We use  $\mathbf{I}_{V^{\text{app}}} \subset \mathbf{I}^{\text{ant}}$  to denote the subset of images that are annotated with  $V^{\text{app}}$  as the ground-truth appearance.

**Construction of the sub-AoG for each appearance candidate:** Based on (7), we can mine the sub-AoG for each appearance candidate  $V^{\text{app}}$ , which uses this appearance's own annotations on images  $I \in \mathbf{I}_{V^{\text{app}}} \subset \mathbf{I}^{\text{ant}}$ , as follows. 1) We first enumerate all possible latent patterns corresponding to the  $k$ -th CNN conv-layer ( $k = 1, \dots, K$ ), by sampling all pattern locations *w.r.t.*  $D_{V^{\text{lat}}}$  and  $\bar{\mathbf{P}}_{V^{\text{lat}}}$ . 2) Then, we sequentially compute  $\hat{\mathbf{P}}_{V^{\text{lat}}}$  and  $\text{Score}(V^{\text{lat}})$  for each latent pattern. 3) Finally, we select a total of  $n_k$  latent patterns with top-ranked values of  $\text{Score}(V^{\text{lat}})$  as  $V^{\text{app}}$ 's children.

## Experiments

### Implementation details

We chose the 16-layer VGG network (VGG-16) (Simonyan and Zisserman 2015) that was pre-trained using the 1.3M

Table 1: Average children number

AoG Layer	#1 semantic part	#2 appearance candidate	#3 latent pattern	#4 CNN unit
Children number	3	4575.8	136.4	–

images in the ImageNet ILSVRC 2012 dataset (Deng et al. 2009) for object classification. Then, given a target category, we used images in this category to fine-tune the original VGG-16 (based on the loss for classifying target objects and background). VGG-16 has 13 conv-layers and 3 fully connected layers. We chose the last 9 (from the 5-th to the 13-th) conv-layers as valid conv-layers, from which we selected units to build the AoG.

Note that during the learning process, we applied the following two techniques to further refine the AoG model. First, multiple latent patterns in the same conv-slice may have similar positions  $\bar{P}_{V^{\text{lat}}}$ , and their deformation ranges may highly overlap with each other. Thus, we selected the latent pattern with the highest  $Score(V^{\text{lat}})$  with each small range of  $\epsilon \times \epsilon$  in this conv-slice, and removed other nearby patterns to obtain a sparse AoG structure. Second, for each  $V^{\text{app}}$ , we estimated  $n_k$ , i.e. the best number of latent patterns in conv-layer  $k$ . We assumed that scores of all the latent patterns in the  $k$ -th conv-layer follow the distribution of  $Score(V^{\text{lat}}) \sim \alpha \exp[-(\text{rank})^{0.5}] + \gamma$ , where  $\text{rank}$  denotes the score rank of  $V^{\text{lat}}$ . We found that when we set  $n_k = \lceil 0.5/\beta \rceil$ , the AoG usually had reliable performance.

## Datasets

We tested our method on three benchmark datasets: the PASCAL VOC Part Dataset (Chen et al. 2014), the CUB200-2011 dataset (Wah et al. 2011), and the ILSVRC 2013 DET dataset (Deng et al. 2009). Just like in most part-localization studies (Chen et al. 2014), we also selected six animal categories—*bird, cat, cow, dog, horse, and sheep*—from the PASCAL Part Dataset for evaluation, which prevalently contain non-rigid shape deformation. The CUB200-2011 dataset contains 11.8K images of 200 bird species. As in (Branson, Perona, and Belongie 2011; Simon, Rodner, and Denzler 2014), we regarded these images as a single bird category by ignoring the species labels. All the above seven categories have ground-truth annotations of the *head* and *torso/back*. Thus, for each category, we learned two AoGs to model its *head* and *torso/back*, respectively.

In order to provide a more comprehensive evaluation of part localization, we built a larger object-part dataset based on the off-the-shelf ILSVRC 2013 DET dataset. We used 30 **animal** categories among all the 200 categories in the ILSVRC 2013 DET dataset<sup>4</sup>. We annotated bounding boxes for the *heads* and *front legs/feet* in these animals as two common part concepts for evaluation. In Experiments, we annotated 3–12 boxes for each part to build the AoG, and we used the rest images in the dataset as testing images.

## Two experiments on multi-shot learning

We applied our method to all animal categories in the above three benchmark datasets. We designed two experiments to

test our method in the scenarios of  $(1 \times 3)$ -shot learning and  $(4 \times 3)$ -shot learning, respectively. We applied the learned AoGs to part localization based on (1) for evaluation.

**Exp. 1, three-shot AoG construction:** For each part concept of an object category, we manually defined three different appearance candidates. We annotated a single bounding box for each appearance candidate. Thus, we used a total of three annotations to build the AoG for this part.

**Exp. 2, AoG construction with more annotations:** We continuously added more part annotations to check the performance changes. Just as in Experiment 1, each part contains the same three appearance candidates. For each appearance candidate, we annotated four parts in four different object images to build the corresponding AoG.

## Baselines

We compared our method with the following nine baselines. The first baseline was the fast-RCNN (Girshick 2015). We directly used the fast-RCNN to detect the target parts on objects. To enable a fair comparison, we learned the fast-RCNN by first fine-tuning the VGG-16 network of the fast-RCNN using all object images in the target category and then training the fast-RCNN using the part annotations. The second baseline was the strongly supervised DPM (SS-DPM) (Azizpour and Laptev 2012), which was trained with part annotations for part localization. The third baseline was proposed in (Li et al. 2013), which trained a DPM component for each object pose to localize object parts (namely, PL-DPM). We used the graphical model proposed in (Chen et al. 2014) as the fourth baseline for part localization (PL-Graph). The fifth baseline, namely CNN-PDD, was proposed by (Simon, Rodner, and Denzler 2014), which selected certain conv-slices (channels) of the CNN to represent the target object part. The sixth baseline (VGG-PDD-finetuned) was an extension of CNN-PDD, which was conducted based the VGG-16 network that was pre-fine-tuned using object images in the target category. Because in the scope of weakly supervised learning, “simple” methods are usually insensitive to the over-fitting problem, we designed the last three baselines as follows. Given the pre-trained VGG-16 network that was used in our method, we directly used this network to extract *fc7* features from image patches of the annotated parts, and learned a linear SVM and a RBF SVM to classify target parts and background. Then, given a testing image, the three baselines brutally searched part candidates from the image, and used the linear SVM, the RBF SVM, and the nearest-neighbor strategy, respectively, to detect the best part. All the baselines were conducted using the same set of annotations for a fair comparison.

## Evaluation metric

As mentioned in (Chen et al. 2014), a fair evaluation of part localization requires to remove the factors of object detection. Therefore, we used object bounding boxes to crop objects from the original images as the testing samples. Note that detection-based baselines (e.g. fast-RCNN, PL-Graph) may produce several bounding boxes for the part. Just as in (Chen et al. 2014; Oquab et al. 2015), we took the most

<sup>4</sup>We will publish this dataset when this paper is accepted.

Table 2: Part localization performance. **Please see supplementary materials for comprehensive results for each category in the ImageNet and Pascal datasets.**

		Exp. 1: 3-shot learning				Exp. 2: 12-shot learning		
Dataset		Pascal		ImageNet		Pascal		ImageNet
Part concept		Head	Torso	Head	F-legs	Head	Torso	Head
Center prediction	SS-DPM	35.3	55.7	45.4	40.6	35.3	55.7	56.0
	PL-DPM	22.2	62.1	36.7	23.7	34.6	67.8	42.7
	PL-Graph	29.4	68.6	46.4	29.5	30.7	68.4	49.2
	Fast-RCNN	24.9	52.6	39.0	30.9	43.1	69.1	61.9
	Ours	<b>73.0</b>	<b>87.7</b>	<b>83.2</b>	<b>71.2</b>	<b>75.1</b>	<b>88.5</b>	<b>82.2</b>
Part detection	SS-DPM	1.5	7.8	7.0	5.1	3.4	8.9	18.8
	PL-DPM	1.1	2.1	3.9	1.2	3.1	4.2	6.5
	PL-Graph	8.6	19.8	15.9	6.3	7.0	23.5	25.1
	Fast-RCNN	5.1	10.5	15.5	6.5	15.0	27.7	35.6
	Ours	<b>29.2</b>	<b>50.7</b>	<b>40.1</b>	<b>23.2</b>	<b>34.6</b>	<b>59.5</b>	<b>55.0</b>

Table 3: Normalized distance of part localization. The performance was evaluated using the CUB200-2011 dataset.

		Exp. 1: 3-shot learning		Exp. 2: 12-shot learning	
Part concept		Head	Torso	Head	Torso
fc7+linearSVM		0.2937	0.2489	0.2938	0.2367
fc7+RBF-SVM		0.3431	0.2691	0.3307	0.2539
fc7+NearestNeighbor		0.4177	0.3331	0.4276	0.3200
SS-DPM		0.3120	0.2721	0.2906	0.2481
PL-DPM		0.3666	0.2994	0.3351	0.2617
PL-Graph		0.4195	0.3337	0.4159	0.3319
CNN-PDD		0.3662	0.2091	0.3658	0.2013
VGG-PDD-finetune		0.3716	0.2129	0.3812	0.2011
Fast-RCNN		0.4423	0.3196	0.2259	0.2923
Ours		<b>0.0848</b>	<b>0.1388</b>	<b>0.0758</b>	<b>0.1368</b>

confident bounding box per image as the localization result. Given localization results of a part in a certain category, we used three evaluation metrics. 1) *Part detection*: a true part detection was identified based on the widely used “IOU  $\geq 0.5$ ” criterion (Girshick 2015); the part detection rate of this category was computed. 2) *Center prediction*: as in (Oquab et al. 2015), if the predicted part center was localized inside the true part bounding box, we considered it a correct center prediction; otherwise not. The average center prediction rate was computed among all objects in the category for evaluation. 3) The *normalized distance* in (Simon, Rodner, and Denzler 2014) is a standard metric to evaluate localization accuracy on the CUB200-2011 dataset.

## Results and quantitative analysis

Table 1 lists the average children number of an AoG node at different layers. Fig. 4 shows the positions of the extracted latent pattern nodes, and part-localization results based on the AoGs. Given an image, we also used latent patterns in the AoG to reconstruct the corresponding part concept based on the technique of (Dosovitskiy and Brox 2016), in order to show the interpretability of the AoG.

In Tables 2 and 3, we compared the performance of different baselines. Our method exhibited much better performance than other baselines that suffered from over-fitting problems (e.g. 29.8% vs. 1.0%–12.3%, 40.1% vs. 3.9%–15.9%, 34.5% vs. 3.1%–15.0%, 55.0% vs. 5.9%–35.6% for detection accuracy of the head in different experiments). In Fig. 3, we showed the performance curve when we in-

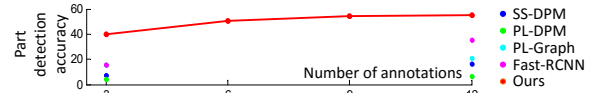


Figure 3: Performance with different numbers of annotations

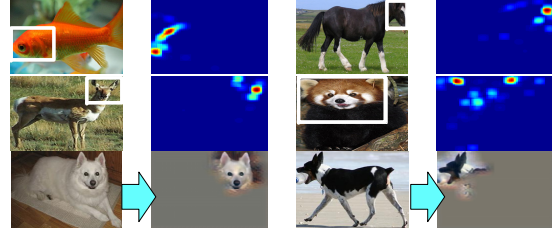


Figure 4: Part localization performance and heat maps corresponding to latent patterns at the 5-th conv-layers in the VGG-16 network (top two rows). In order to demonstrate the AoG interpretability, we reconstructed the dog head using latent patterns in the AoG (bottom row).

creased the annotation number from 3 to 12. Note that the 12-shot learning only improved about 17.4%–37.2% in part detection than 3-shot learning. This demonstrated that our method was efficient in mining CNN semantics, and the CNN units related to each appearance candidate had been roughly mined using just three annotations. In fact, we can further improve the performance by defining more appearance candidates, rather than by annotating more part boxes for existing appearance candidates.

## Conclusions and discussion

In this study, we have explored a probability of incrementally growing new neural connections on a pre-trained CNN to embed new part concepts. Given a temporary demand for modeling a part concept, our method can be conducted with a small number of part annotations (even a single box annotation for each part appearance). In addition, our method semanticizes CNN units by associating them with certain part concepts, and builds an AoG as a white-box model to explain the semantic hierarchy of CNN units.

Because we reduce high-dimensional CNN activations to low-dimensional part/sub-part semantics, our method has high robustness and efficiency in multi-shot learning, and has exhibited superior performance to other baselines.

## Appendix

$$S_I^{\text{inf}}(\mathbf{P}_{V^{\text{app}}} | \hat{\mathbf{P}}_{V^{\text{lat}}}) = -\lambda^{\text{inf}} \min\{\|\hat{\mathbf{P}}_{V^{\text{lat}}} + \Delta\mathbf{P}_{V^{\text{lat}}} - \mathbf{P}_{V^{\text{app}}}\|^2, d^2\}$$

$$S_I^{\text{loc}}(V^{\text{unt}}) = -\lambda^{\text{loc}} \|\mathbf{P}_{V^{\text{unt}}} - \bar{\mathbf{P}}_{V^{\text{lat}}}\|^2$$

$$S_I^{\text{rsp}}(V^{\text{unt}}) = \begin{cases} \lambda^{\text{rsp}} X(V^{\text{unt}}), & X(V^{\text{unt}}) > 0 \\ \lambda^{\text{rsp}} S_{\text{none}}, & X(V^{\text{unt}}) \leq 0 \end{cases}$$

$$S_I^{\text{close}}(V^{\text{lat}}) = -\lambda^{\text{close}} \|\Delta\mathbf{P}_{V^{\text{lat}}}\|^2$$

$$S_I^{\text{pair}}(V^{\text{unt}}) = -\lambda^{\text{pair}} \text{mean}_{V_{\text{upper}}^{\text{lat}} \in \text{Neighbor}(V^{\text{unt}})} \left( \|\mathbf{P}_{V^{\text{unt}}} - \hat{\mathbf{P}}_{V_{\text{upper}}^{\text{lat}}}\| - (\bar{\mathbf{P}}_{V_{\text{upper}}^{\text{lat}}} - \bar{\mathbf{P}}_{V^{\text{lat}}}) \right)$$

where  $X(V^{\text{unt}})$  denotes the normalized response value of  $V^{\text{unt}}$ ;  $d=33$  pxls;  $S_{\text{none}} = -3$  is set for non-activated units.  $\lambda^{\text{inf}}$ ,  $\lambda^{\text{rsp}}$ ,  $\lambda^{\text{loc}}$ ,  $\lambda^{\text{close}}$ ,  $\lambda^{\text{pair}}$  and  $\lambda^{\text{common}}$  are constant weights. We set  $\lambda^{\text{inf}} = 5.0$ ,  $\lambda^{\text{rsp}} = 1.5$ ,  $\lambda^{\text{loc}} = 1/3$ ,  $\lambda^{\text{close}} = 2.0$ ,  $\lambda^{\text{pair}} = 10.0$  and  $\lambda^{\text{common}} = 5.0$  for all categories.

## References

- [Aubry and Russell 2015] Aubry, M., and Russell, B. C. 2015. Understanding deep features with computer-generated imagery. *In ICCV*.
- [Azizpour and Laptev 2012] Azizpour, H., and Laptev, I. 2012. Object detection using strongly-supervised deformable part models. *In ECCV*.
- [Branson, Perona, and Belongie 2011] Branson, S.; Perona, P.; and Belongie, S. 2011. Strong supervision from weak annotation: Interactive training of deformable part models. *In ICCV*.
- [Chen et al. 2014] Chen, X.; Mottaghi, R.; Liu, X.; Fidler, S.; Urtasun, R.; and Yuille, A. 2014. Detect what you can: Detecting and representing objects using holistic models and body parts. *In CVPR*.
- [Darrell 2015] Darrell, D. P. P. K. T. 2015. Constrained convolutional neural networks for weakly supervised segmentation. *In ICCV*.
- [Deng et al. 2009] Deng, J.; Dong, W.; Socher, R.; Li, L.-J.; Li, K.; and Fei-Fei, L. 2009. Imagenet: A large-scale hierarchical image database. *In CVPR*.
- [Dosovitskiy and Brox 2015] Dosovitskiy, A., and Brox, T. 2015. Inverting visual representations with convolutional networks. *In arXiv:1506.02753*.
- [Dosovitskiy and Brox 2016] Dosovitskiy, A., and Brox, T. 2016. Inverting visual representations with convolutional networks. *In CVPR*.
- [Dosovitskiy et al. 2014] Dosovitskiy, A.; Springenberg, J. T.; Riedmiller, M.; and Brox, T. 2014. Discriminative unsupervised feature learning with convolutional neural networks. *In NIPS*.
- [Felzenszwalb, Girshick, and McAllester 2010] Felzenszwalb, P.; Girshick, R.; and McAllester, D. 2010. Cascade object detection with deformable part models. *In CVPR*.
- [Gallagher, Tang, and Tu 2015] Gallagher, P.; Tang, S.; and Tu, Z. 2015. What happened to my dog in that network: unraveling top-down generators in convolutional neural networks. *In arXiv:1511.07125v1*.
- [Ganin and Lempitsky 2015] Ganin, Y., and Lempitsky, V. 2015. Unsupervised domain adaptation in backpropagation. *In ICML*.
- [Girshick 2015] Girshick, R. 2015. Fast r-cnn. *In ICCV*.
- [Krizhevsky, Sutskever, and Hinton 2012] Krizhevsky, A.; Sutskever, I.; and Hinton, G. 2012. Imagenet classification with deep convolutional neural networks. *In NIPS*.
- [Kumaran, Hassabis, and McClelland 2016] Kumaran, D.; Hassabis, D.; and McClelland, J. L. 2016. What learning systems do intelligent agents need? complementary learning systems theory updated. *In Trends in Cognitive Sciences* 20(7):512–534.
- [LeCun et al. 1998] LeCun, Y.; Bottou, L.; Bengio, Y.; and Haffner, P. 1998. Gradient-based learning applied to document recognition. *In Proceedings of the IEEE*.
- [Li et al. 2013] Li, B.; Hu, W.; Wu, T.; and Zhu, S.-C. 2013. Modeling occlusion by discriminative and-or structures. *In ICCV*.
- [Liu, Shen, and van den Hengel 2015] Liu, L.; Shen, C.; and van den Hengel, A. 2015. The treasure beneath convolutional layers: Cross-convolutional-layer pooling for image classification. *In CVPR*.
- [Lu 2015] Lu, Y. 2015. Unsupervised learning on neural network outputs. *In arXiv:1506.00990v9*.
- [Mahendran and Vedaldi 2015] Mahendran, A., and Vedaldi, A. 2015. Understanding deep image representations by inverting them. *In CVPR*.
- [Oquab et al. 2015] Oquab, M.; Bottou, L.; Laptev, I.; and Sivic, J. 2015. Is object localization for free? weakly-supervised learning with convolutional neural networks. *In CVPR*.
- [Si and Zhu 2013] Si, Z., and Zhu, S.-C. 2013. Learning and-or templates for object recognition and detection. *In PAMI*.
- [Simon and Rodner 2015] Simon, M., and Rodner, E. 2015. Neural activation constellations: Unsupervised part model discovery with convolutional networks. *In ICCV*.
- [Simon, Rodner, and Denzler 2014] Simon, M.; Rodner, E.; and Denzler, J. 2014. Part detector discovery in deep convolutional neural networks. *In ACCV*.
- [Simonyan and Zisserman 2015] Simonyan, K., and Zisserman, A. 2015. Very deep convolutional networks for large-scale image recognition. *In ICLR*.
- [Simonyan, Vedaldi, and Zisserman 2013] Simonyan, K.; Vedaldi, A.; and Zisserman, A. 2013. Deep inside convolutional networks: Visualising image classification models and saliency maps. *In arXiv:1312.6034v2*.
- [Szegedy et al. 2014] Szegedy, C.; Zaremba, W.; Sutskever, I.; Bruna, J.; Erhan, D.; Goodfellow, I.; and Fergus, R. 2014. Intriguing properties of neural networks. *In arXiv:1312.6199v4*.
- [Tsogkas et al. 2015] Tsogkas, S.; Kokkinos, I.; Papandreou, G.; and Vedaldi, A. 2015. Deep learning for semantic part segmentation with high-level guidance. *In arXiv:1505.02438v2*.
- [Wah et al. 2011] Wah, C.; Branson, S.; Welinder, P.; Perona, P.; and Belongie, S. 2011. The caltech-ucsd birds-200-2011 dataset. Technical Report CNS-TR-2011-001, In *California Institute of Technology*.
- [Yosinski et al. 2014] Yosinski, J.; Clune, J.; Bengio, Y.; and Lipson, H. 2014. How transferable are features in deep neural networks? *In NIPS*.
- [Zeiler and Fergus 2014] Zeiler, M. D., and Fergus, R. 2014. Visualizing and understanding convolutional networks. *In ECCV*.
- [Zhang, Wu, and Zhu 2015] Zhang, Q.; Wu, Y.-N.; and Zhu, S.-C. 2015. Mining and-or graphs for graph matching and object discovery. *In ICCV*.
- [Zhou et al. 2015] Zhou, B.; Khosla, A.; Lapedriza, A.; Oliva, A.; and Torralba, A. 2015. Object detectors emerge in deep scene cnns. *In ICLR*.
- [Zhou et al. 2016] Zhou, B.; Khosla, A.; Lapedriza, A.; Oliva, A.; and Torralba, A. 2016. Learning deep features for discriminative localization. *In CVPR*.
- [Zhu et al. 2008] Zhu, L.; Chen, Y.; Lu, Y.; Lin, C.; and Yuille, A. 2008. Max-margin and/or graph learning for parsing the human body. *In CVPR*.